6-2022

Fluid pathways in magmatic fluid-dominated hydrothermal system: Upper resurgent cone, Brothers volcano, New Zealand

Esther G. Goita
The University of Southern Mississippi

Fluid pathways in magmatic fluid-dominated hydrothermal system: Upper resurgent cone, Brothers volcano, New Zealand.

by

Esther Gnaridia Goita

A Thesis
Submitted to the Honors College of
The University of Southern Mississippi
in Partial Fulfillment
of Honors Requirements

May 2022

Approved by:

Jeremy Deans, Ph.D., Thesis Advisor,
School of Biological, Environmental and Earth Sciences

Jake Schaefer, Ph.D., Director,
School of Biological, Environmental and Earth Sciences

Sabine Heinhorst, Ph.D., Dean
Honors College

ABSTRACT

The Tonga-Kermadec Arc is an active volcanic arc located between New Zealand and Fiji. The arc expands over an approximate distance of 2530 km. The Kermadec Arc is currently host to over 30 volcanoes, the majority of which are submarine. The magmatic activity along the arc is characterized by the convergence between the Pacific and Australian plates. Brothers volcano is the most active hydrothermal system along the Kermadec arc and hosts two distinct hydrothermal systems, one magmatic fluid dominated, and the other seawater dominated, making the site perfect for studying nascent volcanogenic massive sulfide formation and fluid pathways. The International Ocean Discovery Program (IODP) drilled five sites at Brothers volcano to understand the process of mineral deposit formation from hydrothermal activity and the relationship between discharge of magmatic fluids and the deep biosphere. This project focused on the data acquired from Site U1528, a resurgent cone hosting the magmatic fluid dominated hydrothermal system. Micro computed X-ray tomography (μCT) was used to determine the three-dimensional (3D) pore and secondary mineral structure of seven mini cores from Hole U1528D with varying depth (66.42-297.95 mbsf) and lithology (dacite lapilli tuff to lava flows). The pore characteristics were consistent at this site irrespective of volcanic lithology and depth except for sample 44Z. The total pore volume ranges between 10×10^6 μm^3 and 31×10^6 μm^3. The average pore volume is approximately 1×10^6 μm^3. The variances observed in sample 44Z may be explained by the presence of a vug along a vein in the sample. The data obtained for total number of pores, distribution and volume indicates all rock types in this system have similar characteristics, which may suggest similar eruptive styles and volatile abundance through time. Secondary mineral

phase volume and number have a general increase with depth despite alternating alteration intensity and rock types with depth. A general increase in secondary mineral phases with depth is thought to correlate with increased proximity to the magmatic-derived fluid source and therefore solutes that precipitated out of the fluid. These results indicate the resurgent cone hosts a robust hydrothermal system capable of carrying and precipitating heavy metals. At the Upper Cone, the fluid pathways of magmatic fluids are likely through the bulk rock given the pervasive nature of secondary minerals in all mini cores analyzed. However, outflow at the seafloor suggests there are faster and more voluminous pathways other than pores, like fractures, not studied here.

Keywords: Fluid pathways, magmatic fluids, pores, secondary minerals, alteration, lithology

DEDICATION

"And whatever you do, in word or deed, do everything in the name of the Lord Jesus, giving thanks to God the Father through him." (Colossians 3:17)

This study is wholeheartedly dedicated to the Lord Almighty to whom I owe all in gratitude. To my parents Nyadia Goita and Marthe Diallo, whose strength and dedication are a daily inspiration, in honor of their continuous moral, spiritual, emotional, and financial support.

To my host family, relatives, friends, mentor, and classmates. Thank you all for your continuous support and words of encouragement.

ACKNOWLEDGMENTS

I would like to acknowledge and express immense gratitude to my mentor Dr. Jeremy Deans who relentlessly assisted and guided me throughout the execution and writing process of this thesis project.

Special thanks to the Geology department at The University of Southern Missisippi that equipped me for future success and assisted me in numerous ways throughout my undergraduate studies.

Last but not least, many thanks to the Honors College at The University of Southern Mississippi for their professional and financial assistance.

TABLE OF CONTENTS

LIST OF TABLES

LIST OF ILLUSTRATIONS

LIST OF ABBREVIATIONS

3D	Three-dimentional
CT	Computed Tomography
IODP	International Ocean Discovery Program
mbsf	Meters below seafloor
ROI	Region of interest
UTCT	University of Texas High-Resolution X-ray CT Facility

CHAPTER I: INTRODUCTION

Most caldera systems are poorly exposed leading to the need for numerical models to explain caldera formation and the formation of fluid pathways in hydrothermally active systems (e.g., Stix et al, 2003., Gruehn et al., 2012). In these models, permeability has been assumed to fit surface conditions (i.e., fluid output at the seafloor; Gruehn et al., 2012); however, few natural controls were known or utilized therefore increasing the risk of potential error in these models. Additionally, fluid pathways are unobservable in inactive/ancient volcanic systems. Although high temperature fluids are no longer moving through the system, evidence of fractures, veins, and alteration may be preserved. Calderas, such as Brothers volcano, forming in the back arc of a convergent boundary, tend to form prolific, volcanogenic, polymetallic ore deposits. The high metal content and very acidic fluids in these hydrothermal systems (basaltic to calc-alkaline felsic lavas) are also modern analogues to copper and gold deposits currently and previously mined (Binns et al., 1995). The presence of ores implies economic significance for such research. Consequently, understanding these systems could potentially facilitate exploration and exploitation of various economically significant metals. Knowledge obtained from this project will aid in understanding the Brothers volcano hydrothermal system and other submarine hydrothermal systems both active and inactive.

The Kermadec Arc is currently host to various volcanoes from New Zealand to Fiji, the majority of which are submarine. The magmatic activity along the arc is characterized by the convergence between the Pacific and Australian plates. Brothers volcano hosts the most active hydrothermal system along the Kermadec arc. The volcano

also hosts two distinct hydrothermal systems: on the northwest caldera wall, there is a seawater-dominated system and around a resurgent cone is a magmatic fluid-dominated system. Brothers volcano was the subject of investigation of the International Ocean Discovery Program's Expedition 376. An active, caldera-hosted hydrothermal system had never been drilled to depths below a few meters. Brothers volcano is relatively young and therefore provides a snapshot of a developing volcanogenic, polymetallic ore deposit. The samples and results from Expedition 376, and therefore this study, provide a distinct opportunity to study these systems and in the case of this study, help elucidate how fluids move through these types of systems.

This research focused on seven mini cores obtained from Hole U1528D located in the upper resurgent cone referred to as the Upper Cone. This site is predominantly influenced by magmatic fluids with igneous entities comprised of fresh and altered dacitic rocks, notably, lapillistones, lapilli tephra, dacite lava, and pyroclastic flows (de Ronde et al., 2019A). Hydrothermal fluids are likely to move in 3D with an overall flow upward to lower pressure due to fluid buoyancy. Given the varied volcanic stratigraphy drilled, it would be expected that some units are permeable, leading to more efficient upward or lateral movement. In order to account for patterns of vertical and lateral fluid movement, mini cores were procured in a parallel to the long dimension of the core (Z, vertical) and perpendicular to the long dimension (X, horizontal). Additionally, the number of pores, pore volume, and pore orientation may vary with depth and across lithologies. If these pore networks are interconnected, fluids may preferentially move through certain intervals in certain directions, leading to the focusing of fluids and the potential for the localization of heavy metals. Analysis of fluid pathways in a magmatic

fluid dominated system was conducted through high-resolution X-ray computed tomography (CT) scans, also referred to as micro-CT (μCT). Two distinct thresholds were applied based on density, with the lower density threshold used to identify pore space and the higher density threshold used to identify dense secondary phases (e.g., pyrite, sphalerite). Properties of the pores and secondary mineral phases were analyzed for possible correlations related to depth, porosity, and permeability indicating patterns within the hydrothermal system.

CHAPTER II: GEOLOGIC SETTING

The Kermadec-Tonga arc system is the result of convergence between the Pacific and Australian plates. The arc is approximately 2530 km long and is host to over 94 volcanoes with summit depths ranging from 220 m to 1350 m below sea level (de Ronde et al., 2001). The volcanoes along the Kermadec arc are predominantly submarine. Amongst the observed volcanoes, approximately 35 are estimated to be hydrothermally active. The widespread and dominant hydrothermal activity observed in this area makes it a globally significant source of hydrothermal fluid output. Furthermore the arc system is a significant influence on the oceanic hydrothermal fluxes of heat and mass. The depth of its hydrothermal plumes range from approximately 180 m to1800 m below sea level (de Ronde et al., 2001). Although most of the volcanoes present are volcanic cones, three calderas have been identified, notably, Brothers, Healy, and Rumble II West. Additionally, Brothers and Healy represent the most active venting sites due to the relatively high thickness and distribution of their hydrothermal plumes (de Ronde et al., 2001). The rock composition present along the arc varies between basalt, basaltic andesite, dacite, and rhyodacite (de Ronde et al., 2019A).

Brothers volcano is a hydrothermally active volcanic system located in the Kermadec sector of the Kermadec-Tonga arc located between New Zealand and Fiji. Brothers volcano is the most hydrothermally active volcano within the Kermadec arc system. It is a submarine caldera formed within the Havre Trough, a back arc. Brothers volcano is located ~500 km northeast of Auckland, New Zealand. The caldera has a length of 13 km and a width of 8 km. Its diameter is approximately 3-3.5 km (caldera floor) and the walls of the caldera range from 290 m to 530 m in height. The summit

depth of Brothers volcano is approximately 1350 m below sea level and the base of the caldera occurs at a depth of approximately 2200 m below sea level (de Ronde et al., 2019A). Brothers volcano is comprised of overlapping Upper and Lower Cones, both resurgent cones located in the southeastern part of the caldera. Four active hydrothermal systems and one inactive hydrothermal field are present within the caldera (Embley et al., 2012). Hydrothermal activity actively occurs at the upper caldera, northwest caldera, west caldera, Upper Cone, and Lower Cone. The southeastern rim of the caldera is currently hydrothermally inactive. Brothers volcano is subject to two distinct hydrothermal systems derived from the same magmatic source. The hydrothermal system in the walls of the caldera is predominantly influenced by seawater with a lesser portion of magmatic fluid and a lower fluid to rock ratio. This results in the presence of Cu-Zn-Au rich sulfide chimneys and high temperature (≤320 °C), moderately acidic (pH = 3.2), and gaseous fluids.The resurgent cones in contrast are dominated by magmatic fluid interactions thus, characterized by Fe-oxyhydroxide crusts, native sulfur chimneys, and low temperature (≤120 °C), very low acidity (1.9 pH), and gas-rich fluids (de Ronde et al., 2005, 2011). Previous hydrothermal activity in the area was dominated by magmatic gases and hypersaline brines. A drilling project conducted by Neptune Minerals Inc. in 2005 revealed the presence of hydrothermally altered volcanic rocks ranging from volcanic silt and sand to volcanic glass, gravel, breccia, and more massive volcanic rock along the caldera walls (de Ronde et al., 2019A). These components are overlain by sulfide chimney fragments, glass grit, Fe-Si-Mn oxyhydroxides, and brown ooze. The Upper Cone is comprised of volcanic breccia, gravels, and native sulfur. The overall

composition of Brothers volcano is dominated by dacite and rhyodacite (de Ronde et al., 2019A).

The International Ocean Discovery Program conducted research on Brothers volcano in order to understand the process of mineral deposit formation from hydrothermal activity and the relationship between discharge of magmatic fluids and the deep biosphere. Expedition 376 obtained data from Brothers volcano through five drill sites. Sites U1527 and U1530 are located along the caldera wall, site U1529 is located on the caldera floor, and sites U1528 and U1531 are located on the Upper and Lower resurgent cones. Site U1527 is located at a water depth of 1464 m. The igneous material consists of plagioclase-clinopyroxene-phyric and Fe-Ti oxide–bearing black dacite, scoria, pumice lapilli, lapilli-tuffs, tuff-breccias, and lapillistones (de Ronde et al., 2019A). Site U1529 was located at a water depth of 1765 m. The igneous material consists of plagioclase-pyroxene-phyric dacite lava and monomict lapilli tephra. Site U1530 was located at a water depth of 1595 m. The igneous units at this site consisted of monomict and polymict lapillistones, monomict lapilli-tuff, plagioclase-phyric lava, tuffaceous mudstone, siltstone and sandstone (de Ronde et al., 2019A). Site U1531 is located between the two resurgent cones. This site has igneous units consisting of plagioclase-pyroxene-phyric dacite lava, ash, and lapilli tephra. These units contained plagioclase, orthopyroxene and clinopyroxene phenocrysts and Fe-Ti oxides (de Ronde et al., 2019A).

This project focused on Site U1528, Upper Cone, with a magmatic fluid-dominated hydrothermal system at a water depth of 1228 m. The secondary mineral assemblage at this site is comprised of illite, natroalunite, pyrophyllite, quartz, opal, and

pyrite. The volcanic rocks include plagioclase and pyroxene (de Ronde et al., 2019A). The igneous entities include polymict lapilli tephra, altered lapillistones, lapilli-tuffs, tuff-breccias, dacite lava and pyroclastic rocks.The Upper Cone is characterized by relatively lower temperatures (≤120°C), low pH values, and high gas content. Native sulfur chimneys and Fe oxyhydroxide crusts are observed at this site (de Ronde et al., 2005, 2011)

CHAPTER III: METHODS

Seven mini cores obtained from Hole U1528D were utilized in this study. The mini cores have a diameter varying from 2.40 cm to 2.50 cm and a length varying from 2.30 cm to 3.10 cm. The depths of the cores varied between 66.42 and 297.95 meters below seafloor (mbsf). Letters were attributed to the various cores to indicate the drill direction relative to the overall core obtained from Hole U1528D, Z being parallel to the core and X being perpendicular to the core. Mini cores 3X and 3Z are dacitic lapilli stone with blocks, samples 14Z and 19Z are lapilli tuff and samples 44X, 44Z and 51X are dacitic lava flows.

High-resolution X-ray Computed Tomography (CT) scans of the mini cores were conducted by the University of Texas High-Resolution X-ray CT Facility (UTCT). A NSI scanner was utilized with a Fein focus high power source and voltage of 150kV. In addition to the scanner, an aluminum filter and Perkin Elmer X-ray detector were utilized in the scanning process. The beam hardening was corrected by 0.05 and the post-reconstruction ring correction applied was 2. Post-processing was completed by UTCT, then exported as a series of tif files with an average of approximately 1500 slices per sample at a step size of approximately 20 μm. The scans of the mini cores were rendered in 3D with the Nikon NIS Elements Advanced Research 4.6 software suite at The University of Southern Mississippi. The edges of the cores were deducted to eliminate edge effects, and a region of interest (ROI) was established for the entire mini core to reduce errors caused by unconformities along the edges of the core and obtain a more accurate representation of the core and the pores. The diameter, elongation, distance, orientation, pitch, sphericity, surface, and volume of the pores and secondary minerals

were determined by establishing thresholds (high-end and low-end) and conducting a 3D object measurement. The thresholds were established to best fit the pores (low-end density) and secondary minerals (high-end density). Low-end density thresholds typically ranged from 0-7200 and high-end thresholds typically ranged 41000-65535.

Sphericity is defined as the similarity of the pores or secondary minerals to a sphere, computed as the ratio of the object surface to the surface of a sphere with matching volume maximum sphericity being 1. Pitch is defined as the angle between the major axis and its projection in the x-y plane in the software reference frame, which is the bottom of the sample. Orientation is the angle (θ) between the x-axis and the projection of the major (M) axis in the x-y plane. Elongation characterizes the object shape. Elongation is calculated as the ratio of the axis lengths:

$$(1) \qquad Elongation = \frac{Major}{(minor1+minor2)/2}$$

The diameter is defined as a feature derived from the volume of a sphere with the same volume as the measured object. Distance is the distance between the centroid of the object and the centroid of the nearest object.

The software produced 3D volume images for the pores and secondary minerals. Secondary minerals were color coded according to isolated objects within the core. For further investigation, the data obtained from 3D measurements in Nikon NIS Elements software suite was exported to Excel and plotted in Matlab to produce histograms with the number of pores on the y-axis and analyzed characteristic on the x-axis.

CHAPTER IV: RESULTS

In this section a description of the general characteristics of the pores and secondary minerals across all mini cores is given. Figures 1 and 2 report scans and 3D images of the cores and their pores and secondary minerals. Each characteristic, including diameter, elongation, distance, orientation, pitch, sphericity, surface, and volume, is then described for each mini core for regions of interest highlighted by a low threshold interpreted as pore space, and for secondary minerals that is highlighted by a high threshold.

Sample	Core Image	3-D Computed Tomography Scan Mini core	Computed Tomography Mini core Slice
1528D-3X **Depth:** 66.42 mbsf Dacite lapilli stone with blocks, intensely altered pervasive	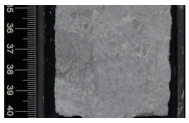	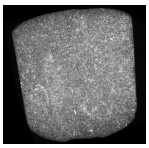	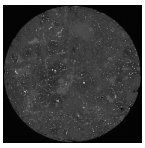
1528D-3Z **Depth:** 66.42 mbsf Dacite lapilli stone with blocks, intensely altered pervasive	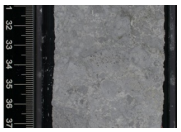	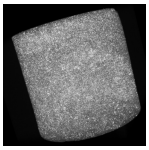	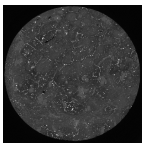
1528D- 14Z **Depth:** 119.64 mbsf Dacite lapilli tuff, intensely altered brecciated	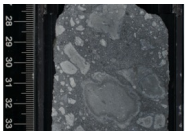	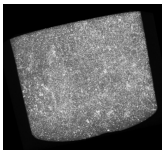	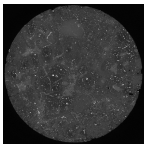
1528D-19Z **Depth:** 145.02 mbsf Dacite lapilli tuff, intensely altered brecciated	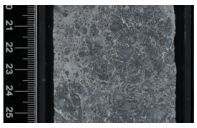	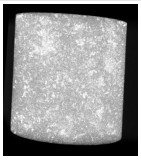	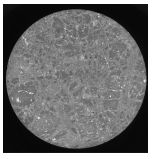
1528D-44X **Depth:** 264.41 mbsf Volcanoclastic lava flow, intensely altered pervasive		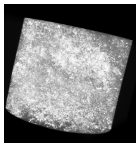	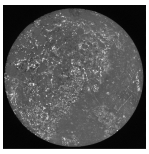
1528D-44Z **Depth:** 264.41 mbsf Volcanoclastic lava flow, intensely altered pervasive	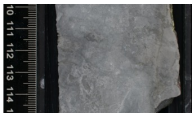	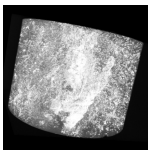	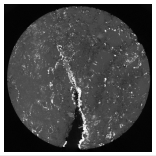
1528D-51X **Depth:** 297.95 mbsf Volcanic lava flow, highly altered pervasive	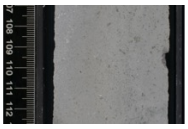	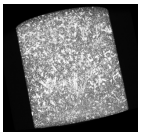	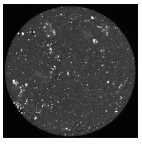

Figure 1: 3-D X-ray computed tomography core images and slices (mini core diameter is 2.5 cm)

Sample	3-D Computed Tomography Scans: Pores (Low end)	3-D Computed Tomography Scans: Secondary Minerals (High end)
1528D-3X Dacite lapilli stone with blocks, intensely altered pervasive	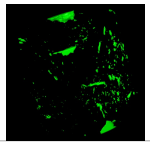	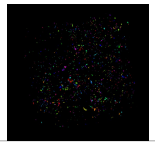
1528D-3Z Dacite lapilli stone with blocks, intensely altered pervasive	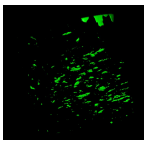	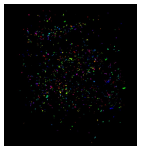
1528D-14Z Dacite lapilli tuff, intensely altered brecciated	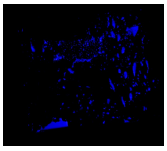	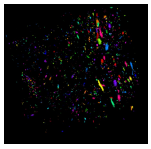
1528D-19Z Dacite lapilli tuff, intensely altered brecciated	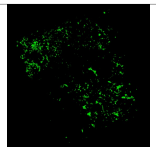	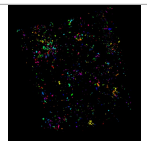
1528D-44X Volcanoclastic lava flow, intensely altered pervasive	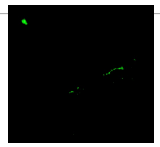	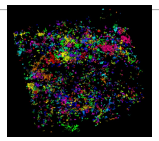
1528D-44Z Volcanoclastic lava flow, intensely altered pervasive	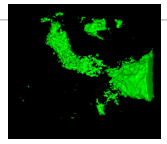	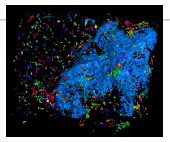
1528D-51X Volcanic lava flow, highly altered pervasive	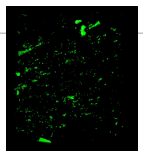	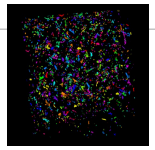

Figure 2: 3-D X-ray computed tomography scans of pores and secondary minerals (mini core diameter is 2.5 cm)

Pores

	Rock Type	Depth [mbsf]	Number of Pores	Total Volume of Pores [μm^3]	Average Pore Volume [μm^3]	Average Pore Elongation	Average Distance [μm]
3X	Lapilli stone with blocks	66.42	7320	10,547,749,102	1,440,162.4	2.07	307.4
3Z	Lapilli stone with blocks	66.42	8239	14,191,621,421	1,721,657.3	2.12	339.9
14Z	Lapilli tuff	119.64	5503	8,851,438,113	1,607,306.7	2.08	325.8
19Z	Lapilli tuff	145.02	41868	31,124,023,355	743,313.5	1.77	297.2
44X	volcanoclastic	264.41	447	886,674,039.6	1,966,017.8	2.2	494.5
44Z	volcanoclastic	264.41	1917	1.52396×10^{11}	79,331,767	2.02	379.6
51X	Lava flow	297.95	31227	31,590,000,147	1,011,527.4	1.87	353.3
Avg.		174.89	13788.71	35,655,358,025	12,545,964.59	2.02	356.81

Table 1: Pore data (lithology, depth, volume, elongation, and distance)

The total pore volume for all samples ranges between 10×10^6 μm^3 and 31×10^6 μm^3. The average pore volume for all samples is approximately 1×10^6 μm^3. The average elongation of the pores (x-axis divided by z-axis) and distance between pores ranges respectively between 1.87 and 2.2 and 297.2 µm and 494.5 µm. Specifics characteristics for each mini core are detailed in the Table 1.

Pore Diameter

For all samples the distribution of pore diameters is overall positively skewed distribution (Figure 3). The majority of the pores irrespective of the lithology have a diameter smaller than 200 µm. The pore diameters among the samples have a maximum ranging from 700-1200 µm with the exception of 44Z, which that has pores with diameters reaching 5000 µm. Considerable similarity in pore diameters was observed between 3X, 3Z, and 14Z.

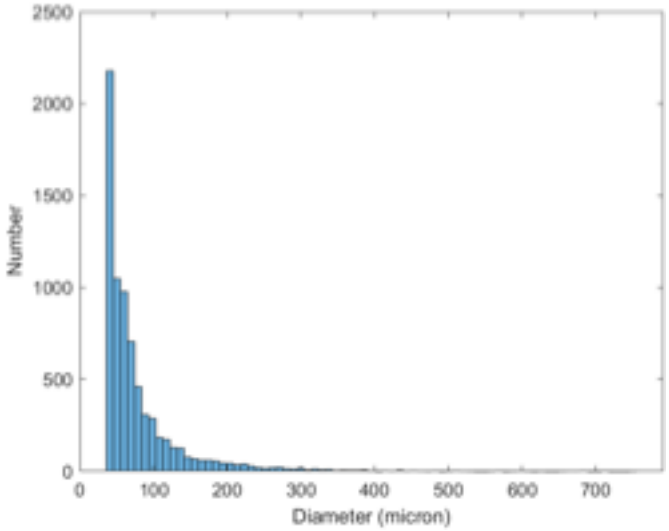

Figure 3: Distribution of the pore diameters for sample 3X

Pore Elongation

The elongation of pores of all the samples is positively skewed (Figure 4). Most of the samples have a maximum elongation of approximately 7 with the exception of samples 14Z and 44X, which had higher values (approximately 12 and 10 respectively), and 51X, which has a lower value (approximately 6).

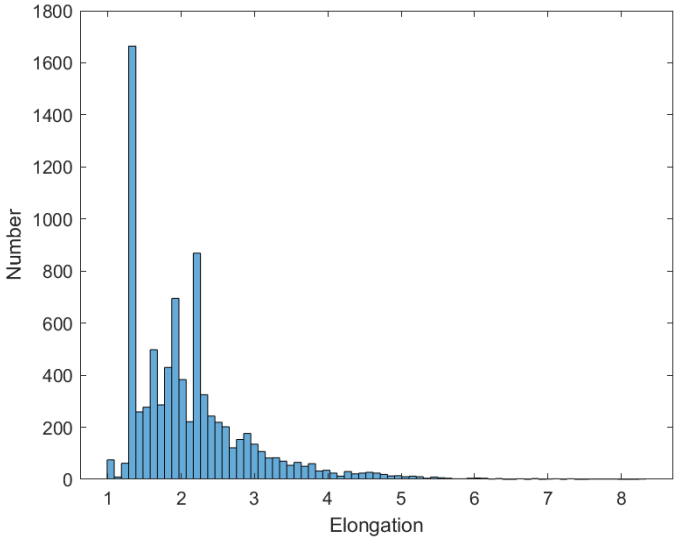

Figure 4: Distribution of the elongation of pores for sample 3Z

Pore Distance and Orientation

The histograms obtained for distance between pores are positively skewed for all samples. Most pores have a distance of 500 μm or lower (Figure 5). The distance between pores varies with the sample with the exception of 3X and 3Z that are relatively identical. Sample 51X has a relatively narrower range and sample 44X has the broadest range. The pore orientations have similar distributions across all the samples. The maximum is approximately 180° with peaks occurring at 0°, 40°, 90°,140°, and 160° (Figure 6).

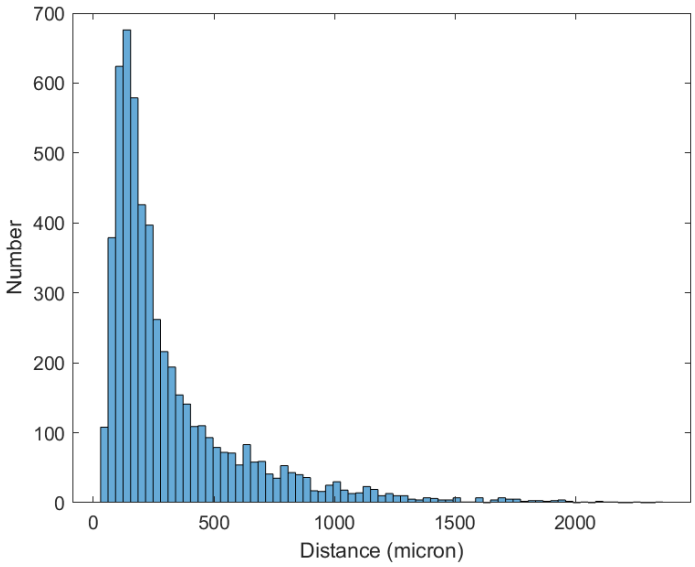

Figure 5: Distribution of the distance between pores of sample 14Z

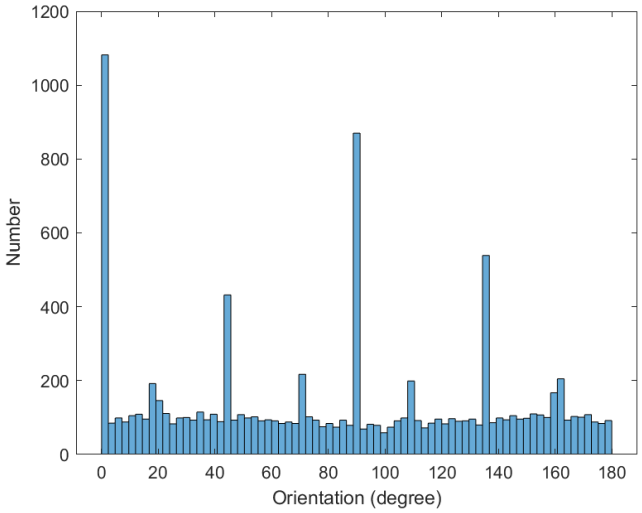

Figure 6: Distribution of the orientation of pores of sample 19Z

Pore Pitch

All samples display a positively skewed data distribution. The results obtained were similar among all mini cores. The maximum value obtained is approximately 90°

with the exception of sample 44X that has maximum of lower by 10° (Figure 7). Mini core 51X had y values (number) reaching 11000 while 44X and 44Z have lower values.

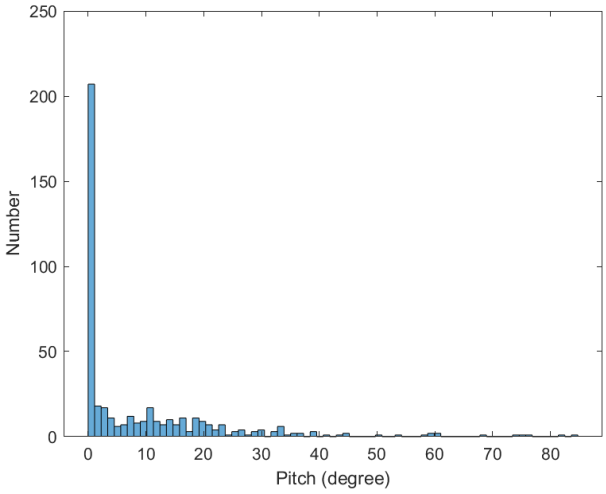

Figure 7: Distribution of the pitch values for pores of sample 44X

Pore Sphericity

The data obtained for pore sphericity had a negatively skewed distribution. The majority of the pores have a sphericity greater than 0.5. The sphericity value 0.8 was the most reoccurring number throughout the mini cores irrespective of lithology (Figure 8).

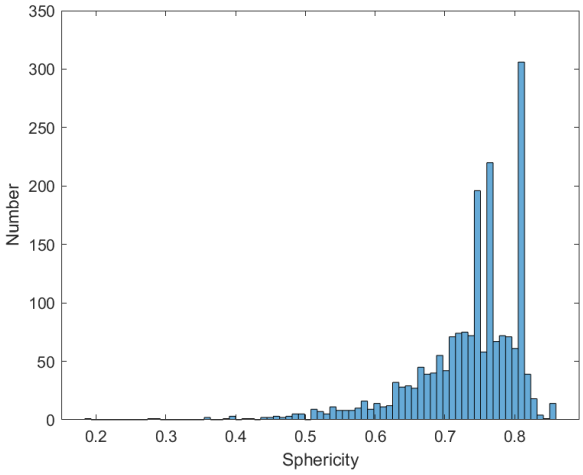

Figure 8: Distribution of the sphericity valuesof pores of sample 44Z

Pore Surface Area and Volume

Pore surface area and volume have similar distributions for all samples. Data obtained for both properties are positively skewed distributions (Figure 9 and 10). Most of the pores have surface area and volume values lower than 0.5 (μm^2 and μm^3, respectively). The maximum surface area and volume values vary per sample. Similarities are observed among 3X and 3Z.

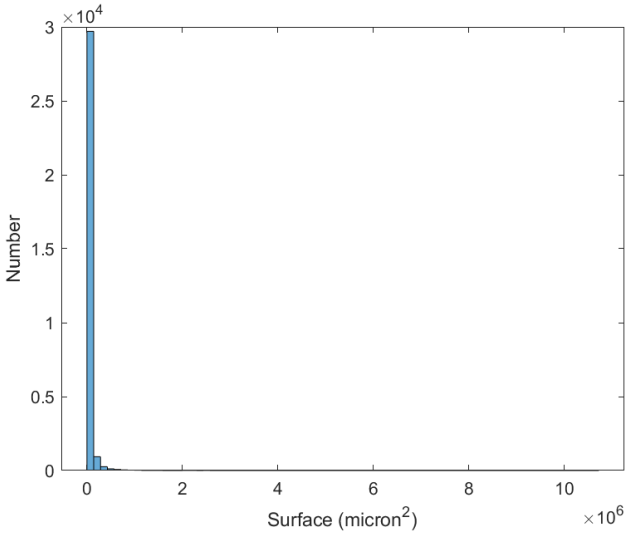

Figure 9: Distribution of the surface areas of pores of sample 51X

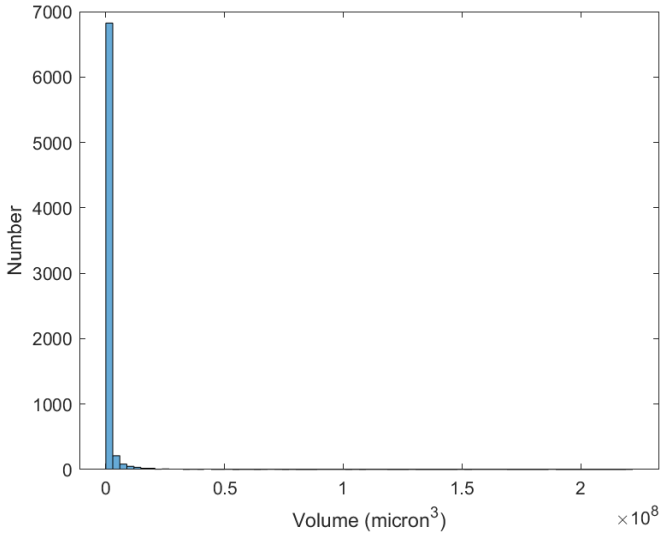

Figure 10: Distribution of the volumes of pores of sample 3X

Secondary Minerals

The total secondary mineral volume ranges between 25×10^{9} μm^3 and 20×10^{10} μm^3. The average elongation and distance between pores range respectively between 1.63 and 1.88 and 223.21 μm and 364.3 μm. Specific data for each mini core are detailed in Table 2.

	Rock Type	Depth [mbsf]	Number of Secondary Minerals	Total Volume of Secondary Minerals [μm^3]	Average Secondary Mineral Volume [μm^3]	Average Secondary Mineral Elongation	Average Secondary Mineral Distance [μm]
3X	Lapilli stone with blocks	66.42	65535	28,614,584,411	436,630.57	1.63	240.92
3Z	Lapilli stone with blocks	66.42	65535	35,309,658,330	538,790.8	1.67	238.27
14Z	Lapilli tuff	119.64	61129	25,397,238,608	415,442.4	1.64	256.07
19Z	Lapilli tuff	145.02	41868	31,124,023,355	743,313.51	1.76	297.16
44X	volcanoclastic	264.41	65535	1.14129×10^11	1,741,492.72	1.87	223.21
44Z	volcanoclastic	264.41	44506	2.05884×10^11	4,625,565.08	1.88	255.87
51X	Lava flow	297.95	38720	76,276,433,916	1,969,745.7	1.82	364.3
Avg.		174.89	54689.71	39,344,387,724	1,495,854.40	1.75	267.97

Table 2: Secondary mineral data (lithology, depth, volume, elongation, and distance)

Secondary Mineral Diameter

The distribution obtained is positively skewed in all samples with most of the minerals having a diameter smaller than 200 μm (Figure 11). There is no consistency between samples of the same lithology. Sample 44Z had considerably greater values relative to the other mini cores, which can be explained by the presence of a vug.

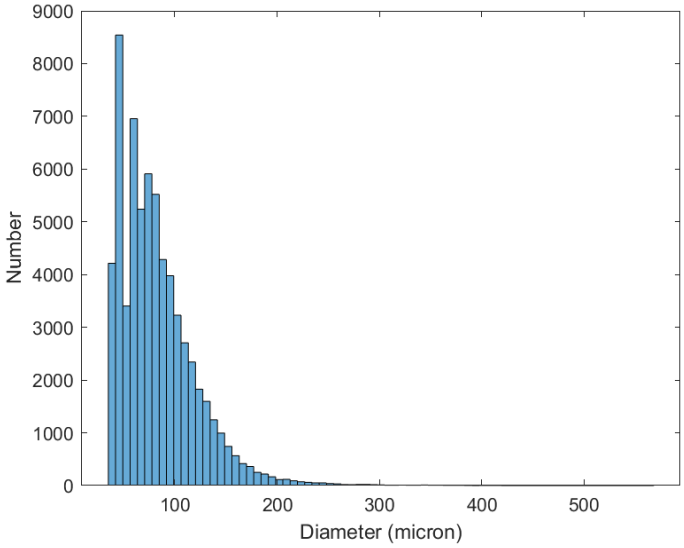

Figure 11: Distribution of the diameter of secondary minerals of sample 3Z

Secondary Mineral Distance

Although the distance histograms are positively skewed, 51X has more symmetrical secondary mineral distance data distribution. No other patterns were observed (Figure 12).

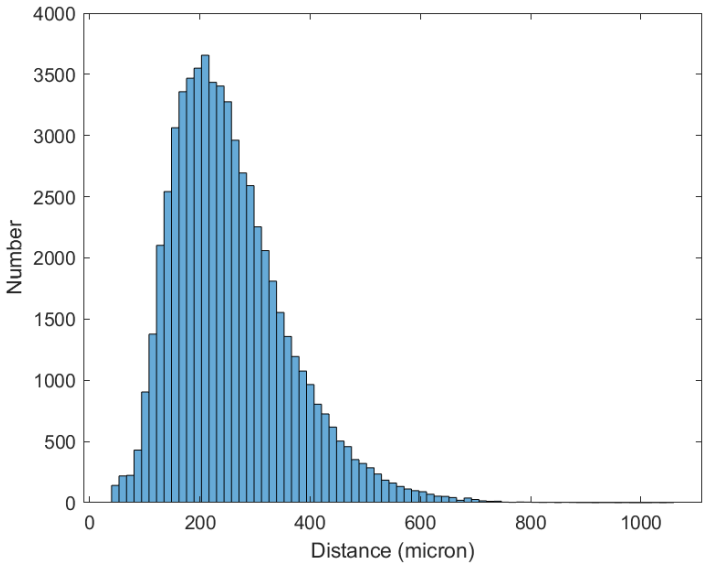

Figure 12: Distribution of the distance between secondary minerals of sample 14Z

Secondary Mineral Orientation and Pitch

These distributions are very similar to those observed for the pores with a maximum at approximately 180° and with peaks occurring at 0°, 40°, 90°,140°, and 160° (Figure 13). The pitch results obtained are positively skewed with a maximum pitch of approximately 90° (Figure 14). There is considerable resemblance between the distributions of samples 3Z and 14X and samples 44X and 44Z. However, the observed numbers (y values) differ. This resemblance in pitch could be due to lithological similarities.

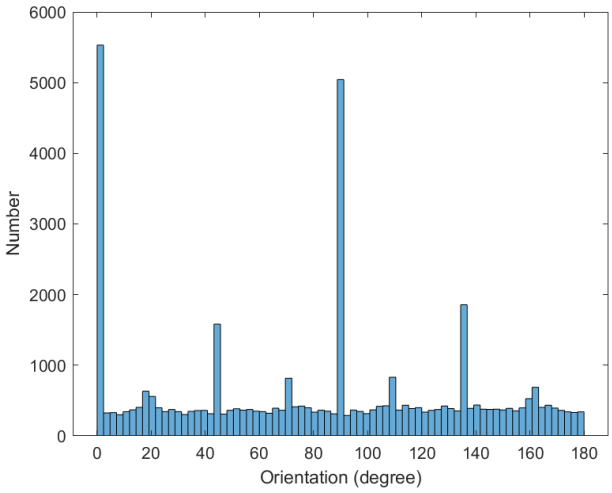

Figure 13: Distribution of the orientations of secondary minerals of sample 19Z

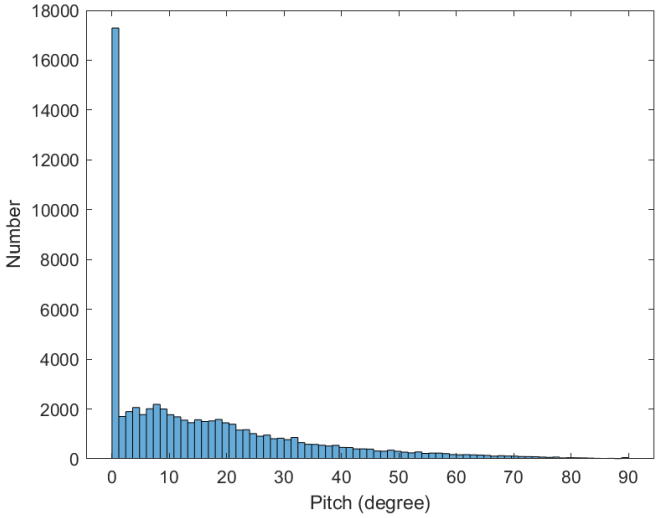

Figure 14: Distribution of the pitch values of secondary minerals of sample 44X

Secondary Mineral Sphericity, Elongation, Surface, and Volume

Similar to the results obtained for pores sphericity, the data distribution of secondary mineral sphericity is negatively skewed (Figure 15). The greatest peaks occur at values higher than 0.7 irrespective of lithology. The elongation distributions are also

positively skewed (Figure 16). The maximum elongation varies between 7 and 10. Furthermore, surface area and volume results are positively skewed (Figures 17 and 18, respectively).

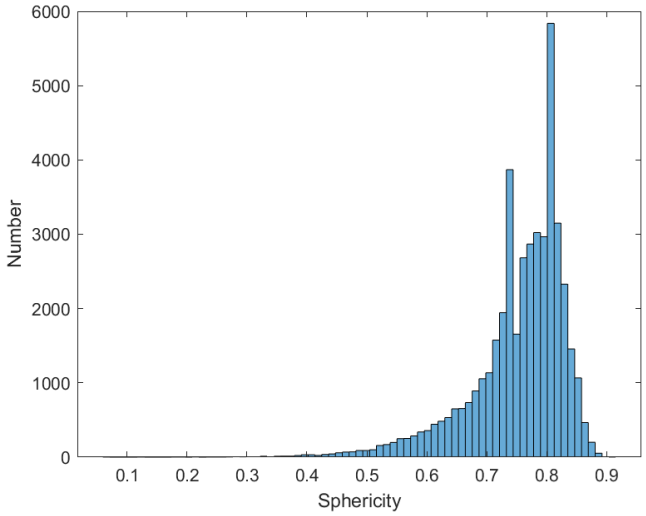

Figure 15: Distribution of the sphericity values of secondary minerals of sample 44Z

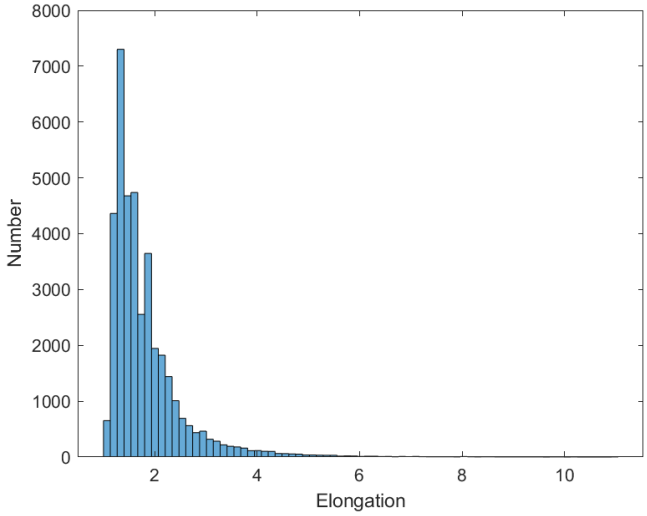

Figure 16: Distribution of the elongation of secondary minerals of sample 51X

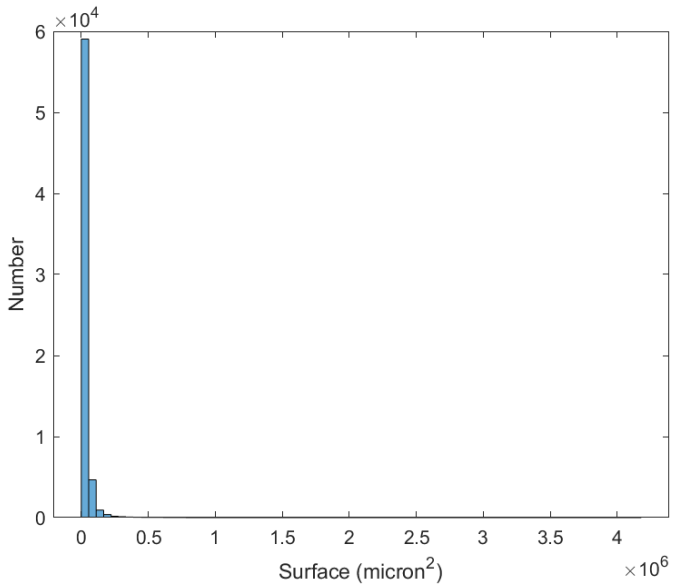

Figure 17: Distribution of the surface area values of secondary minerals of sample 3X

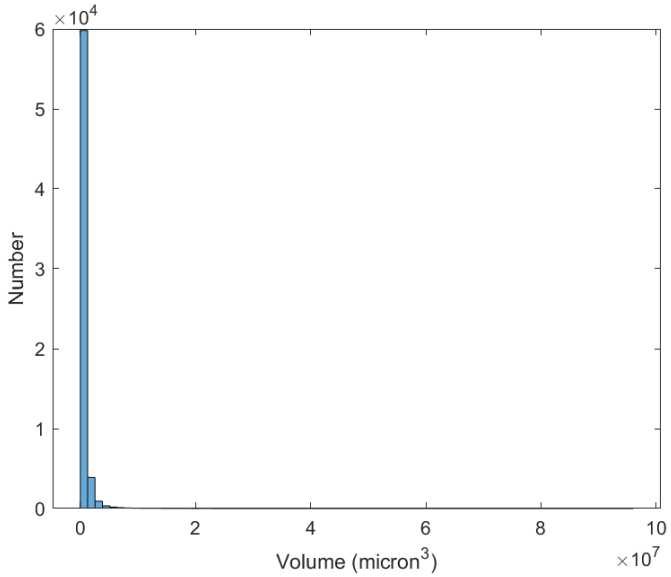

Figure 18: Distribution of the volume of secondary minerals of sample 3Z

CHAPTER V: DISCUSSION

In this section the main results are explained including pore and secondary mineral characteristics (diameter, distance, diameter, elongation, pitch, and sphericity). A comparison is made with results from a study of a similar hydrothermal system in the Pacmanus Basin and other hydrothermal flow pathway models.

Pores

All volcanic rocks at Brothers volcano recovered during Expedition 376 have a dacitic composition (de Ronde et al., 2019B), however, they range from lava flows to pyroclastic, so their pore structures are is not expected to be the same. Lava flows most likely have pores from gas bubbles, forming vesicles. Pyroclastic rocks most likely have pores from the eruptive process defined by grain size and to some extent vesicles. Compaction may also play a role in pore structure since the weight of subsequent eruptions could compact the pore space. An higher presence of pores would be expected to be more apparent in pyroclastic rocks since they are less indurated compared to lava flows.

Surprisingly the pores within the samples analyzed expressed unexpected similarities irrespective of lithology. The pore diameters of all samples fell within a range of 700-1200 microns, which may indicate some uniformity within the system. Such similarities are also observed in other pore characteristics, notably pore distance, diameter, elongation, pitch, and sphericity. The differences observed between pyroclastic rocks and lava flows (sample 51X) may indicate a fundamental control on eruptive style and pore formation with pores within pyroclastic rocks controlled by grain size. Some of

the differences in pore characteristics may be explained by the general increase in secondary minerals at the expense of the pores with depth.

Mini core 44Z is an outlier in terms of pore characteristics, which may be explained by the presence of a vug that runs through most of the core. Sample 44X is also an outlier in this trend with a broader range of distances range between individual pores, which may be explained through the lower number of pores within this sample.

Since most volcanic rocks are porous, it was expected that the pore volume, shape, and orientation may play a role in how fluids move through a sample, with the additional expectation that the pore characteristics would be distinct for each volcanic unit and with depth. The overall low porosity content and similarities in pore characteristics suggest that pores are likely not a controlling factor of fluid pathways in the Upper Cone. This is also reflected in the alteration pattern observed in Hole U1528D with alternating zones recording lower temperature (<300°C) and neutral pH, and higher temperature (~335°C) and low pH (<4) irrespective of lithology (de Ronde et al., 2019). This study also shows that secondary minerals are pervasive (see below) and not limited to pore space. Given these results, the fluids moving through the system, especially the higher temperature and lower pH fluids, are thought to move through the bulk rock rather than preferentially through certain intervals and/or lithologies along porous networks.

Secondary Minerals

The secondary mineral characteristics, similarly to those of pores, reflect no consistency related to lithology. There is a remarkable overall similarity observed between samples 3Z and 14Z, which may be explained by their shared drill orientation (parallel to the main core). The difference in secondary mineral distance between samples

44X and 44Z (wider range) relative to the other samples can be related to conditions at the depth at which those cores were obtained.

Secondary mineral phase volume and number have a general increase with depth. A general increase in secondary mineral phases with depth is thought to correlate with increased proximity to the magmatic-fluid source, which is the source of the chemical components needed to form the secondary minerals i.e., sulfur (Roberts et al, 2003).

Similar observations were made in the Pacmanus system in the Manus basin which has similar composition, but a different tectonic setting. The study conducted at that site portrayed a change in strontium and sulfur isotopes with depth that suggested that magmatic fluids were indeed fluxing into the above volcanic superstructure and that the signal increased with increasing proximity to the magma source, i.e., depth (Roberts et al, 2003). However, Roberts et al. (2003) showed that the magmatic fluid signal is often weak and overprinted by seawater. Additionally, Roberts et al. (2003) suggested that magmatic fluid input and pathways are difficult to track and change through time.

It is likely that the more recent eruptive history in the Upper Cone is indicative that a magma chamber is at a shallower level leading to higher temperature, lower pH fluids that can traverse through the bulk rock by reactive porous flow. Reactive porous flow is a process in which fluids react with the host rock. As a result of this process above the front there is no alteration and behind the front the bulk rock is leached due to exchange with the fluid. This exchange leads to precipitation of secondary minerals. The leaching process could create new pore spaces, that are then filled with secondary minerals. Since secondary minerals are pervasively distributed through all samples, it is clear that hydrothermal fluids have reacted with all intervals drilled. However, given the

alternating pattern of the alteration types, more seawater-dominated fluids most likely have overprinted the higher temperature, lower pH signature. Given the caldera system, it is expected that larger structures are present like faults and fractures, which likely indicates these are the controlling fluid pathways that have led to the alternating patterns of alteration type and the outflow of hydrothermal fluids on the seafloor.

It is expected that some lithologies would have lower porosity and permeability, but this study shows that proximity to the magma chamber (i.e., deeper) is the main control on the number and density of secondary minerals.

Porosity and Permeability

Porosity values for samples 3X, 3Z, 44X, 44Z, and 51X range between 20%-40% (unpublished data), which is one to two orders of magnitude higher than the porosity calculated from the CT scans in this study. The deionized water permeability of the samples ranged between 10^{-18} to 10^{-15} m^2 (unpublished data). These results were similar to those obtained by Iturino et al. (2003) utilizing permeability, electrical resistivity, and X-ray computed tomography measurements, and by Christiansen and Iturrino (2004) on the Pacmanus system. The highest values for permeability are obtained closer to the surface and a general decrease is observed with depth. Christiansen and Iturrino (2004) suggested that this trend is due to alteration. Increased alteration is believed to result in increased correlation between porosity and permeability. Christiansen and Iturrino (2004) suggested that this correlation observed in altered rocks can be explained through the removal of igneous minerals during the alteration process which would create a dependence between porosity, permeability, and alteration. Any further variability amongst the samples may be explained by the difference in alteration types (II and III)

throughout the system (de Ronde et al., 2019B). Considering that alteration is highly related to the proximity to the magma source this further indicates that the main control within the system is related to depth and proximity to the magma source.

CHAPTER VI: CONCLUSION

Brothers volcano hosts the most active hydrothermal system along the Kermadec arc and two distinct hydrothermal systems making the site perfect for studying nascent volcanogenic massive sulfide formation and fluid pathways. Pore characteristics within the analyzed mini cores are very similar across different lithologies and with depth. The general increase of secondary minerals with depth likely indicates increased magmatic fluid input, therefore greater proximity to the magma source. The variation of alteration intensity indicates complex fluid pathways where seawater has likely infiltrated and overprinted higher temperature, lower pH zones at some depths, but not others. Consequently, based on the data obtained it was concluded that the fluid pathways of magmatic fluids at the Upper Cone are likely proceed through the bulk rock given the pervasive nature of secondary minerals in all mini cores analyzed. However, outflow at the seafloor suggests there are faster and more voluminous pathways like fractures, not studied here.

REFERENCES

Binns, R.A., Parr, J.M., Scott, S.D., Gemmell, J.B., and Herzing, P.M., 1995, An active seafloor hydrothermal field on siliceous volcanic rocks in the eastern Manus Basin, Papua New Guinea: Australian Institute of Mining and Metallurgy, v. 95, p. 49-54.

Christiansen, L.B., and Iturrino, G.J., 2004, Core-scale permeability of an actively venting, felsic-hosted hydrothermal system: the PACMANUS hydrothermal field, http://www-odp.tamu.edu/publications/193_SR/202/202.htm (accessed March 2022).

de Ronde, C.E.J., Baker, E.T., Massoth, G.J., Lupton, J.E., Wright, I.C., Feely, R.A., Greene, R.R., 2001, Intra-oceanic subduction-related hydrothermal venting, Kermadec volcanic arc, New Zealand: Earth and Planetary Science Letters, v. 193, i. 3-4, p. 359-369.

de Ronde, C.E., Hannington, M.D., Stoffers, P., Wright, I.C., Ditchburn, R.G., Reyes, A.G., Baker, E.T., Massoth, G.J., Lupton, J.E., Walker, S.L., Greene, R.R., Soong, C.W., Ishibashi, J., Lebon, G.T., et al., 2005, Evolution of a submarine magmatic-hydrothermal system: Brothers Volcano, Southern Kermadec Arc, New Zealand: Economic Geology, v. 100, p. 1097–1133, doi: 10.2113/gsecongeo.100.6.1097.

de Ronde, C.E., Massoth, G.J., Butterfield, D.A., Christenson, B.W., Ishibashi, J., Ditchburn, R.G., Hannington, M.D., Brathwaite, R.L., Lupton, J.E., Kamenetsky, V.S., Graham, I.J., Zellmer, G.F., Dziak, R.P., Embley, R.W., et al., 2011, Submarine hydrothermal activity and gold-rich mineralization at Brothers

Volcano, Kermadec Arc, New Zealand: Mineralium Deposita, v. 46, p. 541–584, doi: 10.1007/s00126-011-0345-8.

de Ronde , C.E.J., Humphris, S.E., Höfig, T.W., Brandl, P.A., Cai, L., Cai, Y., Caratori Tontini, F., Deans, J.R., Farough, A., Jamieson, J.W., Kolandaivelu, K.P., Kutovaya, A., Labonté, J.M., Martin, A.J., et al., 2019 (A), Expedition 376 summary: Brothers Arc Flux, doi: 10.14379/iodp.proc.376.101.2019.

de Ronde, C.E.J., Humphris, S.E., Höfig, T.W., Brandl, P.A., Cai, L., Cai, Y., Caratori Tontini, F., Deans, J.R., Farough, A., Jamieson, J.W., Kolandaivelu, K.P., Kutovaya, A., Labonté, J.M., Martin, A.J., et al., 2019 (B), Site U1528: Brothers Arc Flux, doi: 10.14379/iodp.proc.376.104.2019.

Embley, R.W., De Ronde, C.E.J., Merle, S.G., Davy, B., Tontini, F.C., 2012, Detailed morphology and structure of an active submarine arc caldera: Brothers volcano, Kermadec Arc: Economic Geology, v. 107, p. 1557–1570.

Gruen, G., Weis, P., Driesner, T., de Ronde, C.E., and Heinrich, C.A., 2012, Fluid-flow patterns at Brothers volcano, Southern Kermadec arc: Insights from geologically constrained numerical simulations: Economic Geology, v. 107, p. 1595–1611, doi: 10.2113/econgeo.107.8.1595.

Iturrino, G.J., Ketcham, R.A., Christiansen, L., and Boitnott, G., 2004, Data report: Permeability, resistivity, and X-Ray computed tomography measurements in samples from the PACMANUS hydrothermal system, http://www-odp.tamu.edu/publications/193_SR/205/205.htm (accessed March 2022).

Roberts, S., Bach, W., Binns, Vanko, D.A., et al, 2003, Contrasting evolution of hydrothermal fluids in the PACMANUS system, Manus Basin: The Sr and S isotope evidence: Geology, v. 31, p. 804-808.

Stix, J., Kennedy, B., Hannington, M., Gibson, H., Fiske, R., Mueller., W., Franklin, J., 2003, Caldera-forming processes and the origin of submarine volcanogenic massive sulfide deposits: Geology, v. 31, p. 375–378.